Rarefactive lattice solitary waves with high-energy sonic limit

Anna Vainchtein[*]

Department of Mathematics, University of Pittsburgh, Pittsburgh, Pennsylvania 15260, USA

We compute rarefactive solitary wave solutions in a nonlinear lattice with nearest-neighbor interaction forces that are sublinear near the undeformed state. This setting includes bistable bonds governed by a double-well potential. In contrast to the prototypical Korteweg–de Vries–type delocalization, the obtained solutions feature a nontrivial sonic limit (Chapman-Jouguet regime) with nonzero energy and algebraic decay at infinity. In the bistable case the waves are strongly localized and have high energy over the entire velocity range. Direct numerical simulations suggest stability of the computed solitary waves. We consider several quasicontinuum models that mimic some features of the obtained solutions, including the nontrivial nature of the sonic limit, but fail to accurately approximate their core structure for all velocities in the bistable regime.

I. INTRODUCTION

Since the pioneering studies [1,2] of the Fermi-Pasta-Ulam (FPU) problem that have revolutionized the nonlinear science, there has been a considerable interest in understanding the properties of nonlinear waves in discrete Hamiltonian systems and the extent to which they can be captured by dispersive continuum models. Among the large body of work on this topic that has emerged over the past six decades much attention has been devoted to lattice solitary waves, traveling pulses that carry energy through the system and have been experimentally observed in various settings, including electrical networks [3,4], granular materials [5,6], mechanical metamaterials [7–10], and lipid monolayers [11]. Most theoretical studies of solitary waves in FPU lattices, from the earlier work on the integrable Toda lattice [12] to more recent investigations of such waves in generic nonintegrable lattices, have either considered convex interaction potentials or focused on solutions confined to the convex region. In particular, existence of supersonic solitary waves in FPU lattices with superquadratic potentials was proved in [13,14] and these results were later extended in [15] to potentials with saturable nonlinearity. Small-amplitude solitary waves and their connection to the integrable Korteweg–de Vries (KdV) system near the sonic limit, where the low-energy waves delocalize to zero, was rigorously investigated in [16–22]. The hard-sphere limit of high-energy waves was studied in [23–25]. To obtain solitary wave solutions away from these asymptotic limits in the original FPU problem and its various extensions, numerical [26–29], quasicontinuum [30–38], and asymptotic [39–43] methods have been developed for fully nonlinear potentials, and Fourier transform techniques have been used to construct solutions in lattices with piecewise linear interaction forces [44–47].

In this work we investigate rarefactive solitary waves in a nonlinear lattice with interaction forces that are sublinear near the undeformed state. Of particular interest in this class of problems are bistable lattices with an interaction potential that has two convex regions separated by a nonconvex (spinodal) one, so that its derivative is nonmonotone, as depicted in Fig. 1. Such bistable interactions, with the two convex regions corresponding to different phases, are typically used to model phase transitions in crystals [48–55], biological macromolecules, and polymers [56–58]. Most studies of the nonlinear waves arising in the Hamiltonian systems of this type have focused on spatially extended traveling waves representing shock waves, cracks, and subsonic phase boundaries [50,53,55,59–64]. While existence of solitary waves in bistable lattices has been proved in [65], there have been few systematic investigations of their properties until very recently. In [66,67] the authors employ a combination of impact-induced numerical simulations and exact solutions of quasicontinuum models for three-parabola nonconvex potentials to identify two dimensionless parameters that determine the shape of the wave. Semianalytical solitary wave solutions in a chain with biparabolic bistable interactions have been constructed in [46]. While much insight can be gained from considering piecewise quadratic models, the greater analytical transparency such models provide comes at a cost of certain degeneracies. In particular, velocity of the solitary waves in this setting is bounded from above as well as below, which is not a generic feature in nonlinear lattices. More importantly, as the lower sonic limit is approached, the energy of the waves tends to infinity in both convex [44] and nonconvex cases [46,67] due to delocalization of the solutions to nonzero values at infinity. Meanwhile, in fully nonlinear lattices the limiting energy equals zero in the case of KdV-type delocalization [16] and, as we will show, is finite but nonzero for rarefactive waves considered here. Finally, the waves tend to be wider in lattices with piecewise linear interaction forces, so that quasicontinuum approximations such as the ones employed in [66,67] are closer to the corresponding solutions of
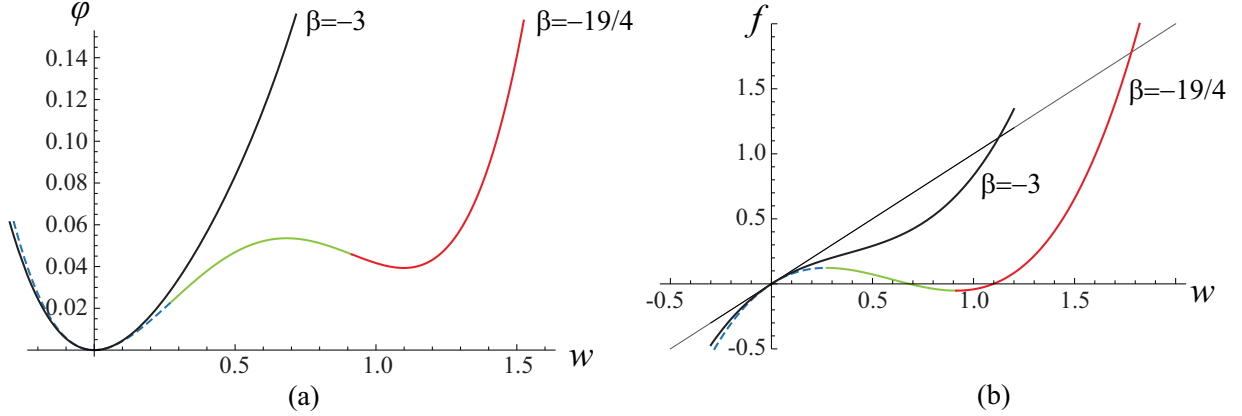
---

[*]aav4@pitt.edu

FIG. 1. (a) Quartic potentials $\phi(w)$ and (b) their derivatives $f(w)$ given by (3), with parameters satisfying (4) at $\alpha = 4$ and different values of β. At $\beta = -19/4$ the parameters also satisfy (5), and the potential is nonconvex. The blue (dashed) and red (dark gray) parts of the $\beta = -19/4$ curves correspond to the two phases, and the spinodal region is marked by green (light gray). The thin straight line through the origin in (b) has unit slope.

the discrete problem than they might be in the fully nonlinear case.

Motivated by these considerations, we use the spectral numerical method developed in [27] to compute rarefactive solitary waves in a fully nonlinear FPU lattice governed by a cubic interaction force with a negative quadratic coefficient. When the magnitude of the coefficient is sufficiently large, the interactions become bistable. Direct numerical simulations initiated by the obtained solutions show steady propagation with the same velocity and suggest their stability. The most interesting feature of the computed solutions, brought about by the sublinearity of the interaction force near the undeformed state, is the *nontrivial sonic limit*, a localized wave with nonzero amplitude and finite energy that features an algebraic decay at infinity. This sonic regime is an analog of the Chapman-Jouguet detonation in the theory of shock waves [68–70]. The nontrivial sonic limit is in stark contrast with the typical scenario for locally convex potentials, where the wave's delocalization to zero in the sonic limit is well described by the KdV solitons [16,21]. Moreover, in the case of bistable interactions, rarefactive solitary waves are strongly localized and carry high energy for all velocities, far from the KdV regime.

To further understand these results and the extent to which they can be captured in a continuum setting, we consider two local quasicontinuum models that have been investigated in detail in [35] for fully nonlinear potentials and used to construct approximate solutions in [66,67] in the piecewise quadratic case. Both models are based on the Padé expansions of the Fourier image of the discrete operator. The first approximation, originally suggested by Collins [30] and Rosenau [33], yields a simple explicit solution that can be directly expanded to obtain the sonic limit, where the exponential decay at infinity is replaced by an algebraic one. The resulting solitary waves capture some features of the numerical solutions of the discrete problem but have larger amplitude and smaller width. The other model is based on a higher-order expansion and provides solutions that are generally closer to their discrete counterparts but does not yield a simple analytical expression. Its solutions have somewhat smaller amplitude and

larger width compared to the discrete case. The two quasicontinuum models by design capture the near-sonic decay of the lattice solitary wave at infinity. When the quadratic coefficient is sufficiently small, they also provide a good approximation of the core structure of the near-sonic waves, which in this case have small but nonzero amplitude. However, when the magnitude of the coefficient becomes sufficiently large, including the case of bistable interactions, solutions obtained from the quasicontinuum models deviate from their discrete counterparts in the core region over the entire velocity interval due to the strong localization of the waves. These findings suggest that a new paradigm is necessary to describe strongly localized solitary waves in a lattice with bistable interactions.

The rest of the paper is organized as follows. In Sec. II we formulate the problem and discuss parameter bounds. Numerical and asymptotic results for the discrete problem are presented in Sec. III. Quasicontinuum models are analyzed in Sec. IV, which also includes the comparison to the discrete problem and a brief discussion of another model, based on the global approximation of the discrete operator. We summarize and discuss our findings in Sec. V.

II. PROBLEM FORMULATION

Consider an infinite chain of particles with equal masses and nearest-neighbor interactions governed by a nonlinear potential. In terms of dimensionless variables, the total energy (Hamiltonian) of the system is

$$H = \sum_{n=-\infty}^{\infty} \left(\frac{1}{2} \dot{u}_n^2 + \phi(u_n - u_{n-1}) \right), \tag{1}$$

where $u_n(t)$ is the displacement of nth particle, $\dot{u}_n(t) = u_n'(t)$ is its velocity, and $\phi(w)$ is the interaction potential. The equations of motion,

$$\ddot{u}_n = f(u_{n+1} - u_n) - f(u_n - u_{n-1}),$$

where $f(w) = \phi'(w)$ is the interaction force, can be rewritten in terms of the strain variable $w_n = u_n - u_{n-1}$, yielding

$$\ddot{w}_n = f(w_{n+1}) - 2f(w_n) + f(w_{n-1}). \tag{2}$$

In what follows, we assume that upon an appropriate rescaling the potential $\phi(w)$ and its derivative $f(w)$ satisfy the following requirements:

(A1) $\phi(0) = f(0) = 0$ and $f'(0) = 1$;

(A2) $f''(0) < 0$;

(A3) $f'(w) > 1$ for large enough $w > 0$.

The conditions (A2) and (A3) are needed for the existence of homoclinic orbits corresponding to sonic and supersonic rarefactive solitary waves, as discussed below. Note that (A1) and (A2) imply that the interaction force $f(w)$ is *sublinear*, $f(w) < w$, for small enough nonzero $|w|$, as illustrated in the right panel of Fig. 1.

Of particular interest is a subclass of potentials that in addition to (A1)–(A3) satisfy the following condition:

(A4) there exist $w_- > 0$ and $w_+ > w_-$ such that $f'(w_-) = f'(w_+) = 0$, $f'(w) > 0$ for $w < w_-$ and for $w > w_+$, while $f'(w) < 0$ for $w_- < w < w_+$.

This means that the potential is *nonconvex* inside the *spinodal region* (w_-, w_+). The convex regions $w < w_-$ and $w > w_+$ can represent two different material phases, phase I and phase II, respectively. The elastic modulus of phase I corresponding to the homogeneous deformation $w \equiv 0$ is rescaled to unity by (A1).

As a prototypical example of potentials satisfying (A1)–(A3), we consider the cubic interaction force

$$f(w) = \frac{\alpha}{3} w^3 + \frac{\beta}{2} w^2 + w, \qquad (3)$$

where we assume that

$$\alpha > 0, \quad \beta < 0. \qquad (4)$$

For nonconvex potentials satisfying (A4), we also require that

$$\beta^2 - 4\alpha > 0, \qquad (5)$$

which ensures the existence of the spinodal region of width $\sqrt{\beta^2 - 4\alpha}/\alpha$. Examples of convex and double-well potentials satisfying these conditions are shown in Fig. 1.

We now seek solitary wave solutions of (2). These are localized traveling wave solutions of the form

$$w_n(t) = w(\xi), \quad \xi = n - Vt, \qquad (6)$$

where $V > 0$ is the velocity of the wave, so they satisfy the advance-delay differential equation

$$V^2 w'' = f(w(\xi + 1)) - 2f(w(\xi)) + f(w(\xi - 1)) \qquad (7)$$

and vanish at infinity:

$$w(\xi) \to 0 \quad \text{as } |\xi| \to \infty. \qquad (8)$$

We seek positive solutions $w(\xi) > 0$ (rarefactive waves) that are even in ξ, $w(\xi) = w(-\xi)$. Note that the velocity V must satisfy

$$V \geqslant 1, \qquad (9)$$

since the presence of radiation modes at subsonic velocities $0 < V < 1$ generally precludes the formation of solutions satisfying (8) [35]. Under our assumptions on the interaction potential, for $V \geqslant 1$ the straight line emanating from $w = 0$ with the slope V^2 intersects the graph of $f(w)$ at $w = w_* > 0$ satisfying $f(w_*) = V^2 w_*$ and lies above the graph of $f(w)$

between the two points. Here w_* is the center of the homoclinic orbit in the (w, w') plane that corresponds to the solitary wave we are seeking. For bistable potentials satisfying (A1)–(A4), $w = 0 < w_-$ is in phase I and $w_* > w_+$ is in phase II, so the solitary wave connects the two phases.

III. SOLITARY WAVE SOLUTIONS

A. Numerical results

To find solitary wave solution numerically, we use the Fourier spectral method outlined in [27]. We approximate $w(\xi)$ by an L-periodic even function with large enough period L and that can be represented by Fourier cosine series:

$$w(\xi) \approx \sum_{j=0}^{N-1} c_j \cos \frac{2\pi j \xi}{L}, \qquad (10)$$

with collocation points set to be $\xi_i = iL/[2(N-1)]$, $i = 0, \ldots, N-1$. We substitute the series approximation (10) into (7) evaluated at ξ_i, $i = 0, \ldots, N-2$. An additional equation is the trapezoidal approximation (utilizing the collocation points) of

$$V^2 \int_{-\infty}^{\infty} w(\xi) d\xi = \int_{-\infty}^{\infty} f(w(\xi)) d\xi,$$

which is obtained by multiplying (7) by ξ^2 and integrating by parts under the assumption that $w(\xi)$ and $w'(\xi)$ decay sufficiently fast at infinity. This last condition ensures that (8) holds. In the end, we get a system of N nonlinear algebraic equations for N unknown coefficients in (10), which is solved using the trust-region dogleg algorithm in Matlab. We used $L = 160$, $N = 2001$ for most computations and $L = 320$, $N = 4001$ to compute wider waves.

The amplitude-velocity relation for the obtained solutions for the cubic interaction force (3) with $\alpha = 4$ and different values of β satisfying (4) is shown in Fig. 2(a). Here $\beta = -1$ and $\beta = -3$ correspond to convex potentials, while the potentials with $\beta = -19/4$ and $\beta = -21/4$ are bistable ($\beta < -4$ at $\alpha = 4$).

Importantly, when V approaches the sound speed $V = 1$, the solutions tend to a limit with a *nonzero amplitude*. This is illustrated in Fig. 2(b), which shows near-sonic solutions at $V = 1.001$. This limiting behavior is a signature feature of the interaction forces that are sublinear near the origin [see Fig. 1(b)] due to $f''(0) < 0$ and thus prevent homoclinic connections that correspond to small-amplitude rarefactive solitary waves, while supporting such orbits for compressive waves [20]. When they exist, small-amplitude solutions delocalize to zero in the sonic limit and are well described by the KdV equation near this limit [16]. Such an approximation is clearly not valid in this case. At larger $|\beta|$, which includes nonconvex potentials (represented here by examples with $\beta = -21/4$ and $\beta = -19/4$), the solutions are more localized, with smaller width and higher amplitude. As the negative β tends to zero, approaching the case of FPU-β potential with a purely quartic anharmonic term in $\phi(w)$, the sonic limit tends to zero.

The details of the near-sonic solution behavior at larger ξ are shown in Fig. 3, where we also include the case $\beta = -5$. In addition to greater localization at larger $|\beta|$, one can see
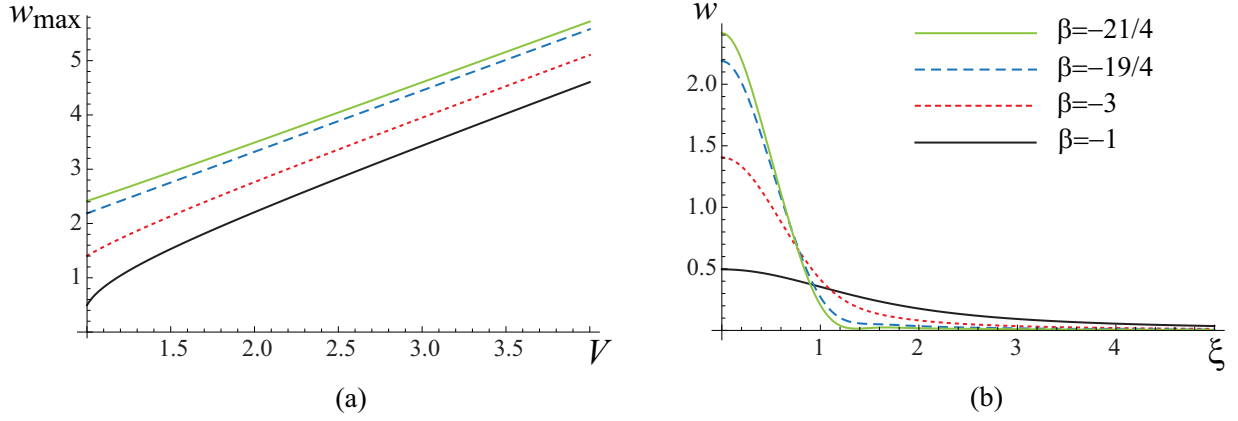
FIG. 2. (a) Amplitude $w_{\mathrm{max}} = w(0)$ of the solitary wave solutions as a function of V at $\alpha = 4$ and different values of β. (b) Solutions near the sonic limit ($V = 1.001$). Due to the even symmetry of solitary wave solutions, only the part with $\xi \geqslant 0$ is shown in this and subsequent figures.

that the combination of the advance-delay terms in (7) and nonmonotonicity of $f(w)$ for bistable potentials results in oscillations of $w'(\xi)$, so that for large enough $|\beta|$ ($\beta = -21/4$ and $\beta = -5$ in the figure) $w(\xi)$ is *nonmonotone* at $\xi > 0$. The oscillatory nature of the solutions, which is not typically observed in lattice solitary waves in the absence of competing interactions [37,45] persists at larger velocities, as shown in the insets of Fig. 4. At fixed β, solutions decay faster at infinity at larger V. At given V, the waves have higher amplitude and are more localized at larger $|\beta|$.

To check the obtained solutions and probe their stability, we ran numerical simulations of (2) in a finite chain of M particles (typically, we set $M = 400$) initialized by the computed solitary wave solutions. Typical results are shown in Fig. 5, where the simulations initialized by the computed solution with $V = 1.2$ and $V = 4$ at $\alpha = 4$, $\beta = -19/4$ yielded steadily propagating solitary waves. Both the solitary wave profile obtained from the numerical simulations and their velocities differ from the computed ones by $O(10^{-8})$ and $O(10^{-9})$ for $V = 1.2$ and $V = 4$, respectively.

Similar agreement between computed solitary waves and the ones obtained from numerical simulations was found for

all solutions that were probed, with velocities ranging from $V = 1.001$ to $V = 4$, and different values of β. This suggests stability of the computed solitary waves. This observation is consistent with the monotonic increase of their energies H with V, as shown in Fig. 6, and hence nonzero $H'(V)$, a necessary condition for stability [18,71,72].

B. Some asymptotic results

We now derive asymptotic behavior at infinity for the solutions of the discrete problem. To this end, we start by transforming (7) to the Fourier space:

$$V^2 W(k) = \Lambda(k) F(k), \quad \Lambda(k) = \frac{4 \sin^2(k/2)}{k^2}, \quad (11)$$

where k is the wave number and $W(k)$ and $F(k)$ are the Fourier transforms of $w(\xi)$ and $f(w(\xi))$, respectively. Writing $F(k) = W(k) + \mathcal{N}(k)$, where $\mathcal{N}(k)$ is the Fourier transform of the nonlinear contribution to $f(w(\xi))$, we obtain

$$[V^2 - \Lambda(k)] W(k) = \Lambda(k) \mathcal{N}(k).$$

We are interested in the behavior of solutions at large $|\xi|$, where $w(\xi)$ is small. For $V > 1$, we can thus neglect the nonlinear part $\mathcal{N}(k)$, obtaining the characteristic equation
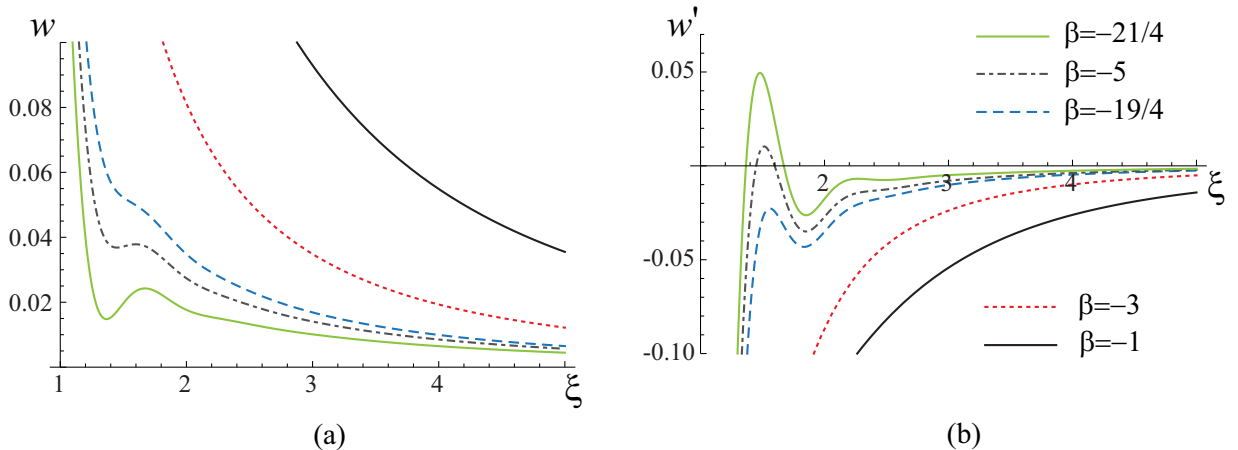

FIG. 3. Detailed view of (a) the near-sonic solution at $V = 1.001$ and (b) its derivative at larger ξ. Here $\alpha = 4$.
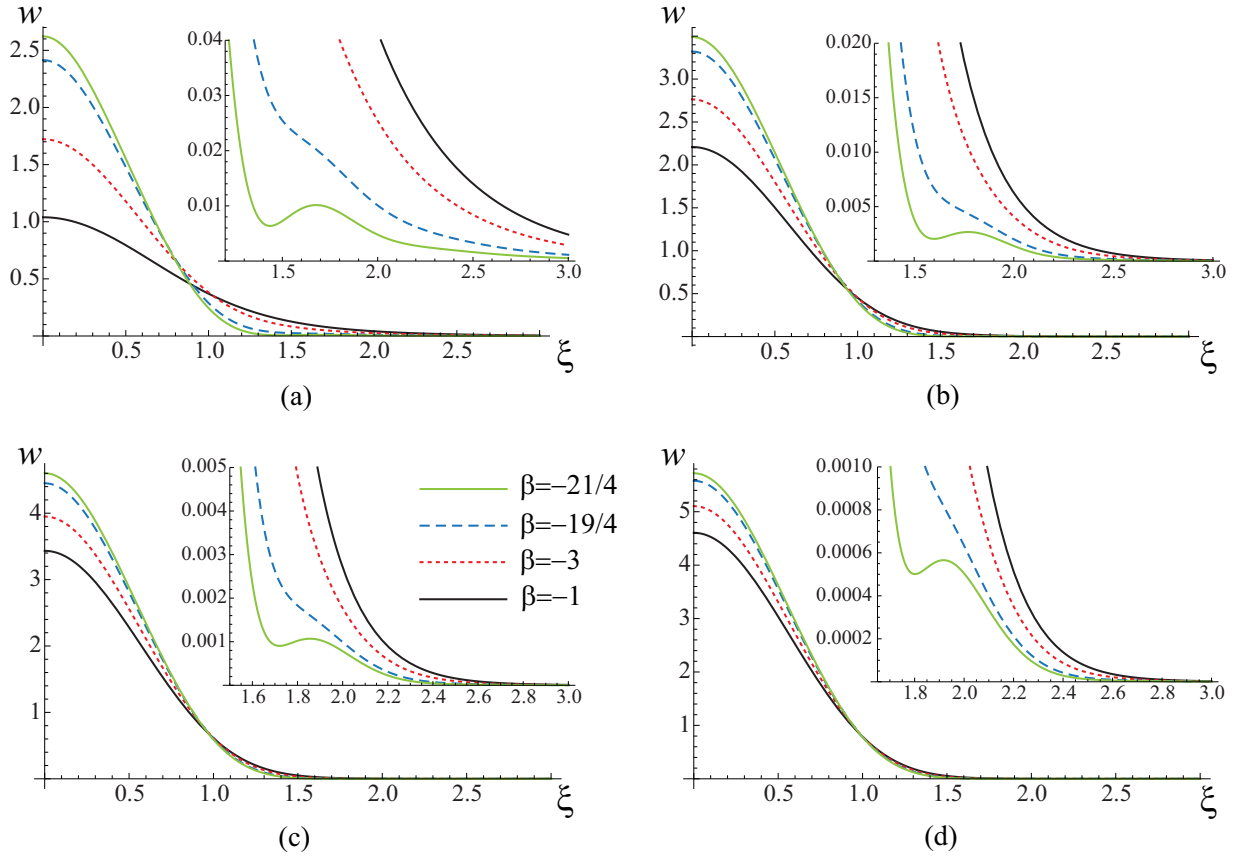
FIG. 4. Solitary wave solutions at $\alpha = 4$ and different values of β with velocities (a) $V = 1.2$, (b) $V = 2$, (c) $V = 3$, and (d) $V = 4$. Insets show the solution behavior at larger ξ.

$V^2 = \Lambda(k)$ for the discrete problem linearized about $w = 0$. This equation has purely imaginary roots $k = \pm ip$ at $V > 1$, where V-dependent $p > 0$ satisfies $2 \sinh(p/2) = V p$. This leads to the exponential decay $w(\xi) \sim e^{-p|\xi|}$ at large $|\xi|$. The decay rate increases with V, in agreement with our numerical findings.

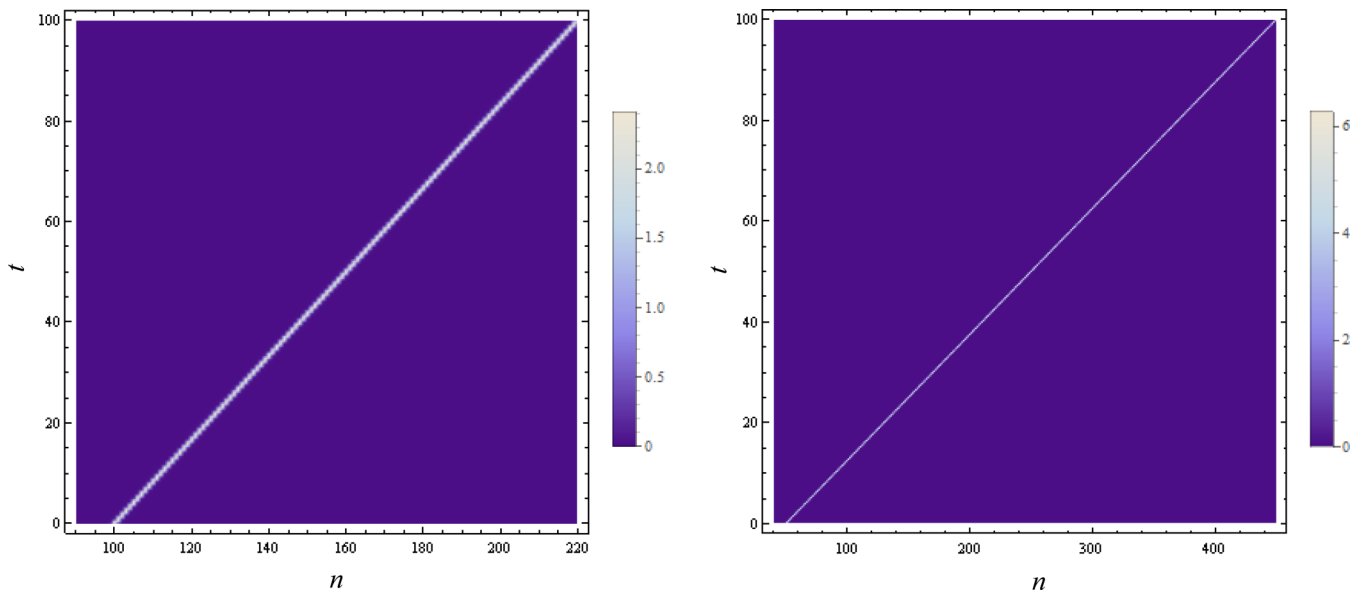
FIG. 5. Space-time plots of $w_n(t)$ from the numerical simulations initialized by the computed solitary waves with (a) $V = 1.2$ and (b) $V = 4$. Here $\alpha = 4$ and $\beta = -19/4$.
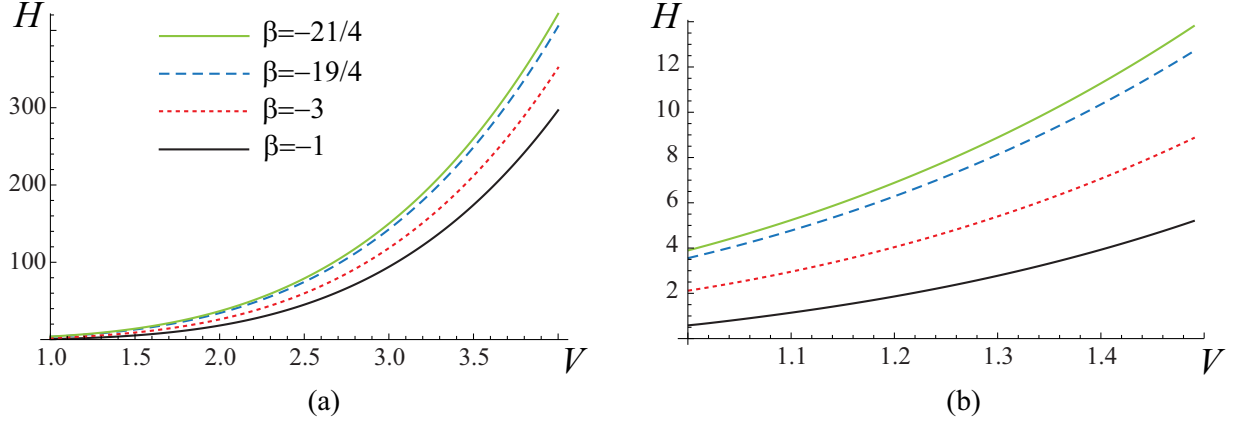
FIG. 6. (a) Energy H of the computed solitary waves as the function of their velocity V at different β. (b) Enlarged view of the plot near the sonic limit.

The sonic limit $V = 1$ needs to be considered separately. In this case we have

$$[1 - \Lambda(k)]W(k) = \Lambda(k)\mathcal{N}(k).$$

For small k (slowly varying solutions), $\Lambda(k) \approx 1 - k^2/12$, so we have

$$\frac{k^2}{12}W(k) \approx \mathcal{N}(k). \tag{12}$$

Consider now the cubic nonlinearity (3), so that $\mathcal{N}(k)$ is the Fourier transform of $(\beta/2)w^2(\xi) + (\alpha/3)w^3(\xi)$. Taking inverse Fourier transform of (12) and neglecting the cubic term under the assumption that $w(\xi) > 0$ is small, we obtain $w'' \approx -6\beta w^2$, which in view of (8) yields

$$w' \approx \pm 2\sqrt{-\beta}\,w^{3/2}. \tag{13}$$

Here we used the fact that $\beta < 0$ [recall (4)], and thus (13) has a nontrivial solution. Hence in the sonic limit the exponential decay of $w(\xi)$ at infinity is replaced by an *algebraic* one:

$$w \approx -\frac{1}{\beta\xi^2} \quad \text{as } |\xi| \to \infty. \tag{14}$$

We emphasize that this nonlinear effect is due to the sublinearity of $f(w)$ near the origin, which is imposed by $\beta < 0$, and the fact that we consider rarefactive waves. When $\beta \geqslant 0$, such waves have small amplitude at near-sonic velocities and tend to $w \equiv 0$ in the sonic limit, and the same is true for compressive waves at $\beta < 0$ [20].

IV. QUASICONTINUUM MODELS

To better understand some of the observations described in the previous section, we now turn to quasicontinuum descriptions that replace the advance-delay differential equation (7) by an ordinary differential equation (ODE). Local quasicontinuum models, based on the expansion of the discrete operator near the long-wave limit, are usually derived under the assumption that the solutions are slowly varying (have a small high-frequency component), which does not hold for tall and narrow solitary waves in discrete chains. Nevertheless, in some cases such models have been shown to capture at least some features of the discrete problem far outside the

regime of their validity [35,44,66,67]. Although, as we have seen, solitary wave solutions we obtained in the discrete case may vary rather rapidly even in the sonic limit, we proceed below to consider two local quasicontinuum approximations of the discrete model. In addition, we will investigate a global approximation that was proposed in [35] and aims to capture the higher frequencies.

Following [35], we consider Padé approximations of $\Lambda(k)$ defined in (11) and use these approximations to replace (7) by an ODE. A comprehensive review of various quasicontinuum models can be found in [35].

A. Collins-Rosenau model

We start by considering the (0,2) Padé approximation of $\Lambda(k)$ in (11), which leads to a model proposed in [30,33] and henceforth referred to as the *CR model*. In this approach we use

$$\Lambda(k) \approx \frac{1}{1 + \frac{k^2}{12}},$$

an $O(k^2)$ approximation of $\Lambda(k)$ near $k = 0$ which yields the second-order ODE

$$V^2 w(\xi) - \tfrac{1}{12}V^2 w''(\xi) = f(w(\xi)). \tag{15}$$

Multiplying both sides of (15) by $w'(\xi)$, integrating, and using the fact that both $w(\xi)$ and $w'(\xi)$ tend to zero at infinity, we obtain

$$\tfrac{1}{2}V^2 w^2(\xi) - \tfrac{1}{24}V^2(w'(\xi))^2 - \phi(w(\xi)) = 0,$$

and thus the homoclinic orbit corresponding to a solitary wave solution with velocity V is described by [35]

$$w' = \pm\frac{2\sqrt{6}}{V}\sqrt{\frac{V^2}{2}w^2 - \phi(w)}. \tag{16}$$

This immediately implies that the amplitude $w_{max} = w(0)$ of the wave and its velocity are related by

$$V^2 w_{max}^2 = 2\phi(w_{max}). \tag{17}$$

The homoclinic orbit goes through the origin and $(0, w_{max})$ point in the (w, w') plane.

In the case of the cubic nonlinearity (3), Eq. (16) can be integrated in quadratures. Indeed, we have

$$\int_{w_{\max}}^{w} \frac{dy}{y\sqrt{1 - \gamma y - \delta y^2}} = \pm \frac{2\sqrt{3(V^2 - 1)}}{V}\xi, \qquad (18)$$

where we define

$$\gamma = \frac{\beta}{3(V^2 - 1)}, \quad \delta = \frac{\alpha}{6(V^2 - 1)}, \qquad (19)$$

and the amplitude of the wave $w_{\max} = w(0)$ is the positive root of $1 - \gamma y - \delta y^2 = 0$:

$$w_{\max} = \frac{\sqrt{\gamma^2 + 4\delta} - \gamma}{2\delta} = \frac{\sqrt{\beta^2 + 6\alpha(V^2 - 1)} - \beta}{\alpha}. \quad (20)$$

Integrating (18) and recalling (19), we obtain

$$w(\xi) = \frac{6(V^2 - 1)}{\beta + \sqrt{\beta^2 + 6\alpha(V^2 - 1)}\cosh\left[\frac{2\sqrt{3}\sqrt{V^2-1}}{V}\xi\right]}. \quad (21)$$

Implicit in these calculations is the assumption that V satisfies (9). Note that in the special cases $\alpha = 0$, $\beta > 0$ and $\alpha > 0$, $\beta = 0$ solution (21) reduces to the rarefactive waves obtained in [26,35].

If $\alpha = 0$, $\beta > 0$ or $\alpha > 0$, $\beta \geqslant 0$, the obtained positive solution tends to zero in the sonic limit when $V \to 1$ from above. This mimics the well-known KdV localization in the sonic limit of the solutions of the lattice solitary waves with such interaction potentials [16]. However, in the case $\alpha > 0$, $\beta < 0$ considered here, $w(\xi)$ has a *nonzero sonic limit* instead. More precisely, a simple Taylor expansion at small $V^2 - 1$ yields

$$w(\xi) = -\frac{2\beta}{\alpha + 2\beta^2 \xi^2} \qquad (22)$$

as the limiting sonic strain profile [recall that $\beta < 0$, and thus $w(\xi) > 0$]. Note that, as in the discrete problem, we have the algebraic decay (14) in this limit. The nonzero amplitude of the limiting solution equals $-2\beta/\alpha$.

B. (2,2) Padé approximation

To obtain a more accurate quasicontinuum model, we now consider (2,2) Padé approximation of $\Lambda(k)$ that we will call the *P22 model*:

$$\Lambda(k) \approx \frac{1 - \frac{1}{20}k^2}{1 + \frac{1}{30}k^2}.$$

This approximation is $O(k^4)$ accurate near $k = 0$ but still yields a second-order ODE:

$$V^2 w(\xi) - \frac{1}{30}V^2 w''(\xi) = f(w(\xi)) + \frac{1}{20}f''(w(\xi))(w'(\xi))^2 + \frac{1}{20}f'(w(\xi))w''(\xi). \qquad (23)$$

Taking into account the fact that w and w' vanish at infinity, one can obtain the first integral [35]

$$\tfrac{1}{2}[2V^2 + 3f'(w(\xi))]^2(w'(\xi))^2 - 60V^4 w^2(\xi) - 180V^2 w(\xi)f(w(\xi)) + 300V^2\phi(w(\xi)) + 90[f(w(\xi))]^2 = 0. \qquad (24)$$

This yields the amplitude-velocity relation [35]

$$V^2 = \frac{1}{2w_{\max}^2}\{5\phi(w_{\max}) - 3w_{\max}f(w_{\max}) + \sqrt{10\phi^2(w_{\max}) + 15[w_{\max}f(w_{\max}) - \phi(w_{\max})]^2}\} \qquad (25)$$

for general interaction potential. In the cubic case (3) this yields

$$V^2 = \frac{1}{24}\left(-\left(6 + 8\beta w_{\max} + 7\alpha w_{\max}^2\right) + \sqrt{5}\{180 + w_{\max}[56\beta^2 w_{\max} + 16\beta(12 + 5\alpha w_{\max}^2) + \alpha w_{\max}(132 + 29\alpha w_{\max}^2)]\}^{1/2}\right), \qquad (26)$$

which can be inverted to obtain $w_{\max}$ as a function of V but the resulting expression is too unwieldy to include here.

In the cubic case (3) the first integral (24) yields the homoclinic orbit in the (w, w') plane defined by

$$w' = \pm\frac{\sqrt{5}w}{2V^2 + 3(1 + \beta w + \alpha w^2)}[2V^2(6 + 8\beta w + 7\alpha w^2) + 24V^4 - (6 + 3\beta w + 2\alpha w^2)^2]^{1/2}. \qquad (27)$$

This equation can be solved for ξ as a function of w in terms of elliptic integrals. To ensure the existence of the relevant solution within our parameter bounds, we need to assume that $\alpha > 0$ and $-(1/3)\sqrt{10(3 + 2\sqrt{3})\alpha} < \beta < 0$, which holds for all numerical examples in Sec. III. One can show that, in this case for each V satisfying (9), the fourth-degree polynomial under the square root in (27) has two V-dependent real roots, $w = w_{\max}$ and $w = -e$, where e is strictly positive for $V > 1$ and tends to zero in the limit $V \to 1$. In addition, there are two complex conjugate roots $c \pm id$, where c and d are positive and depend on V. This yields

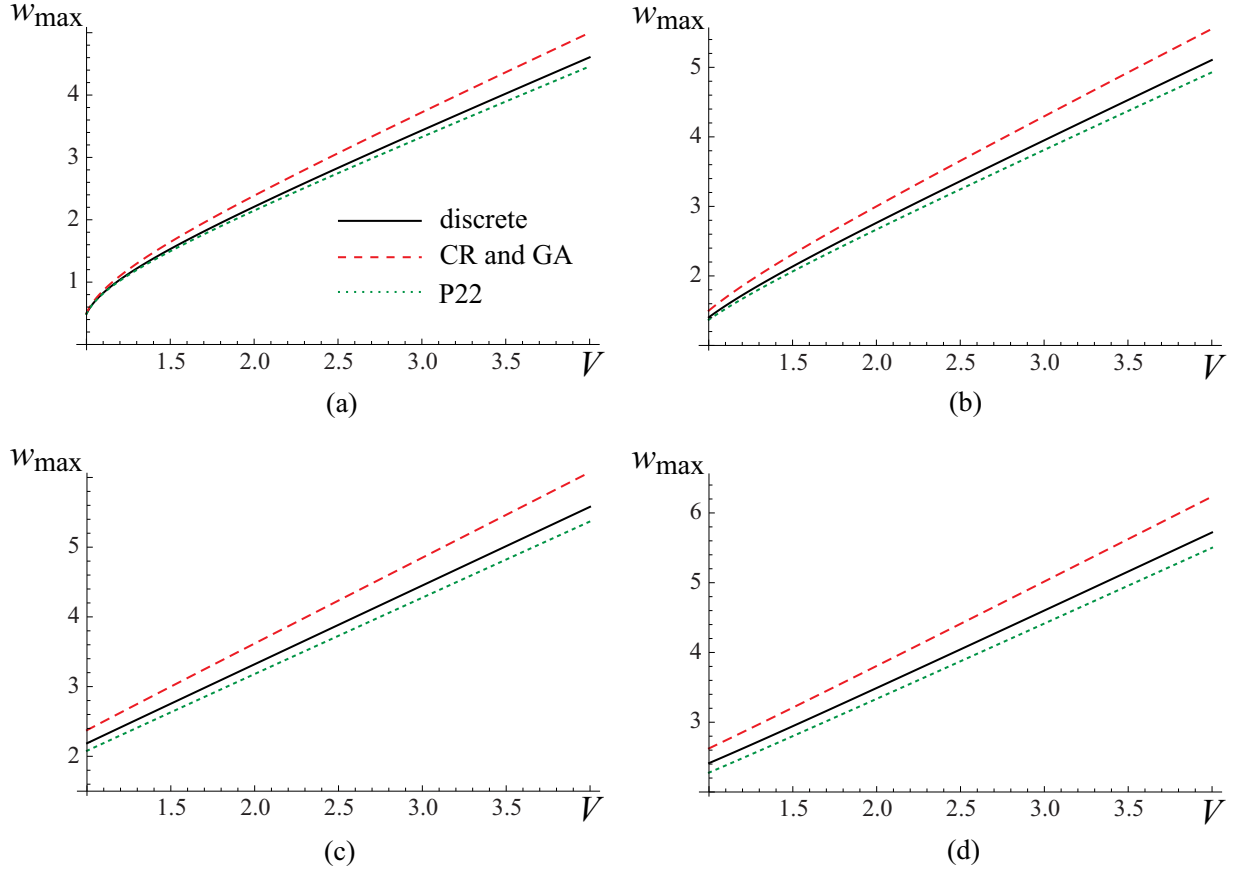$$\xi = \pm\frac{1}{2\alpha\sqrt{5}}[I(w_{\max}) - I(w)], \qquad (28)$$

FIG. 7. Amplitude $w_{max} = w(0)$ of the solitary wave solutions as a function of V for the discrete, CR, P22, and GA models at (a) $\beta = -1$, (b) $\beta = -3$, (c) $\beta = -19/4$, and (d) $\beta = -21/4$. Here $\alpha = 4$.

where

$$
I(y) = \int \frac{2V^2 + 3(1 + \beta y + \alpha y^2)}{y\sqrt{(w_{max} - y)(y + e)[(y - c)^2 + d^2]}} dy
$$

$$
= -\frac{2}{w_{max}} \sqrt{\frac{c - id - w_{max}}{c - id + e}} \left\{ \frac{2V^2 + 3(1 + \beta w_{max} + \alpha w_{max}^2)}{\sqrt{(c - w_{max})^2 + d^2}} F(z(y)|\mu) \right.
$$

$$
\left. + \frac{\sqrt{(c - w_{max})^2 + d^2}}{(c - id)(c + id - w_{max})} \left[3\alpha(c - id)w_{max}\Pi(\nu; z(y)|\mu) - (3 + 2V^2)\Pi\left(\nu\frac{w_{max}}{c - id}; z(y)|\mu\right) \right] \right\}. \tag{29}
$$

Here $F(z(y)|\mu)$ and $\Pi(\nu; z(y)|\mu)$ are elliptic integrals of the first and third kind, respectively, with V-dependent

$$
\mu = \frac{2id(e + w_{max})}{(c - id + e)(c + id - w_{max})}, \quad \nu = \frac{2id}{c + id - w_{max}},
$$

and

$$
z(y) = \arcsin\sqrt{\frac{(c + id - w_{max})(c - id - y)}{2id(w_{max} - y)}}
$$

$$
= \frac{\pi}{4} - i \ln\{\sqrt{2}[\text{Re } \zeta(y) - \text{Im } \zeta(y)]\},
$$

where

$$
\zeta(y) = \frac{1}{\sqrt{2}}\left(1 - i\frac{c^2 + d^2 - c(w_{max} + y) + w_{max}y}{d(w_{max} - y)}\right)^{1/2}.
$$

Unlike the simpler special cases $\alpha = 0$ and $\beta = 0$ considered in [35], the solution (28) cannot be written in terms of elementary functions, and even in those cases inverting the resulting expression to obtain w as a function of ξ requires solving a nonlinear transcendental equation, which in practice calls for an iterative approach [35]. Thus, while the P22 approximation is more accurate than the CR model, it does not yield explicit waveforms even in the case of polynomial nonlinearity $f(w)$.

We remark that, when $\beta < -2\sqrt{5\alpha/3}$, the numerator of the integrand of $I(y)$ in (29) has two zeros, w_1 and $w_2 > w_1$, which correspond to zero $\xi'(w)$, or, equivalently, infinite $w'(\xi)$, for $1 \leqslant V < \sqrt{(3/2)[\beta^2/(4\alpha) - 1]}$. In this case $\xi(w) > 0$ defined by the plus sign in (28) is a nonmonotone function, with a local minimum at w_1 and a local maximum at w_2. This means in this parameter regime solution (28)
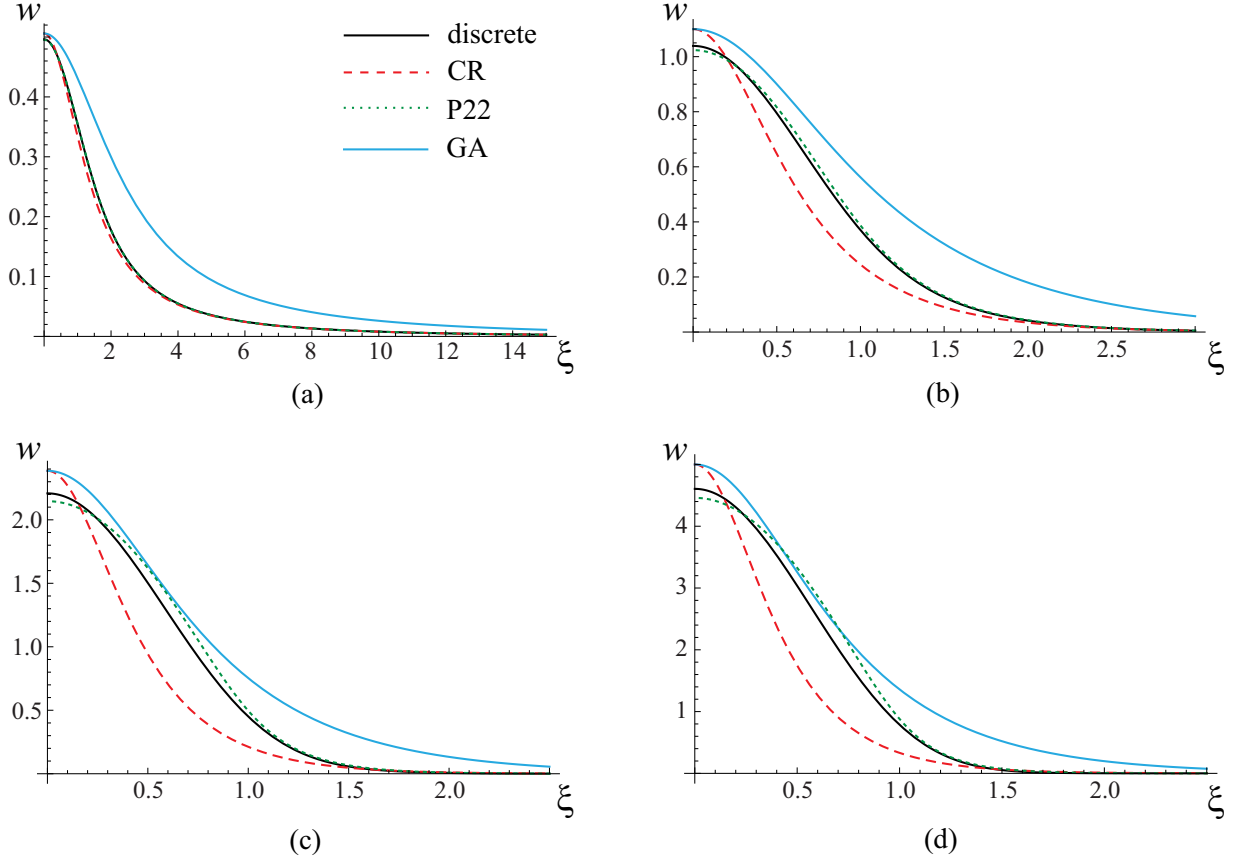
FIG. 8. Strain profiles $w(\xi)$ of the computed solitary wave for the discrete CR, P22, and GA models with (a) $V = 1.001$, (b) $V = 1.2$, (c) $V = 2$, and (d) $V = 4$. Here $\alpha = 4$ and $\beta = -1$.

cannot be inverted to yield a single-valued function $w(\xi)$. Instead, the corresponding profile is triple-valued in the intervals $(\xi(w_1), \xi(w_2))$ and $(-\xi(w_2), -\xi(w_1))$. This is clearly an artifact of the Padé approximation and does not reflect a property of the discrete problem.

We now consider the asymptotic behavior of $w(\xi)$ at infinity. Since w is small at large $|\xi|$, it suffices to expand (27) about $w = 0$. For $V > 1$ this yields

$$w' = \pm \frac{2\sqrt{15}\sqrt{2V^4 + V^2 - 3}}{3 + 2V^2} w + O(w^2), \qquad (30)$$

yielding exponential decay at infinity with the rate that is strictly greater than that of the CR solution (21) for all supersonic velocities:

$$\frac{2\sqrt{15}\sqrt{2V^4 + V^2 - 3}}{3 + 2V^2} > \frac{2\sqrt{3}\sqrt{V^2 - 1}}{V}, \quad V > 1. \quad (31)$$

In the sonic limit $V = 1$ (30) is no longer valid. Instead, we obtain

$$w' = \pm 2\sqrt{-\beta} w^{3/2} + O(w^{5/2}), \qquad$$

which coincides to the leading order with (13) in the discrete case and yields the same algebraic decay (14) as in the discrete and CR models.

C. Global approximation

In addition to the local quasicontinuum models investigated above, which rely on approximating $\Lambda(k)$ in (11) in the small-wavelength region, one could attempt to approximate $\Lambda(k)$ globally over the entire spectrum. Such an approach is considered, for example, in [35], where the author seeks a global approximation of $\Lambda(k)$ in the form $\Omega(k) = 1/(a + bk^2)$ in order to take the advantage of the availability of explicit solutions in this case, and finds that the best approximation is achieved when $a = 1$ and $b = 1/4$, which force $\Omega(0) = \Lambda(0)$ and minimize the L^2 norm of $\Lambda(k) - \Omega(k)$. This sacrifices the accuracy of the approximation at smaller k but improves it at the higher values. As designed, this approach yields the explicit solution

$$w(\xi) = \frac{6(V^2 - 1)}{\beta + \sqrt{\beta^2 + 6\alpha(V^2 - 1)} \cosh\left[\frac{2\sqrt{V^2 - 1}}{V}\xi\right]}, \qquad (32)$$

which has the same amplitude as the CR one but larger width and slower decay at infinity. We will refer to this model as the *GA model* below.

D. Comparison of discrete and quasicontinuum models

We now compare the results of the discrete and quasicontinuum models for the specific examples considered in Sec. III, with fixed $\alpha = 4$ and different negative β values.
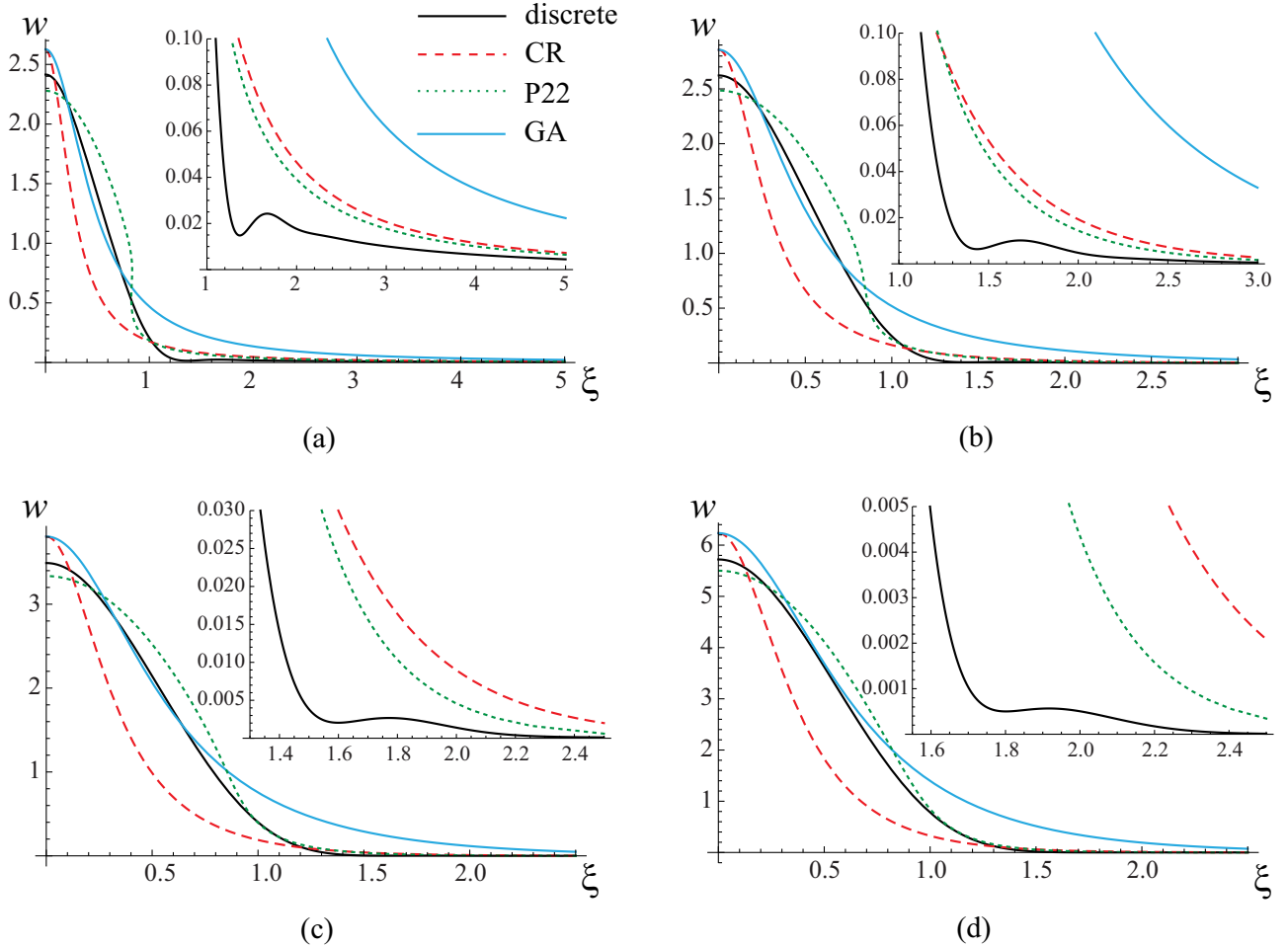
FIG. 9. Strain profiles $w(\xi)$ of the computed solitary wave for the discrete CR, P22, and GA models with (a) $V = 1.001$, (b) $V = 1.2$, (c) $V = 2$, and (d) $V = 4$. Insets show the details of the solutions at larger ξ. Here $\alpha = 4$ and $\beta = -21/4$.

We start by considering the solution amplitudes for the three models shown in Fig. 7. One can see that for each velocity the CR and GA models (dashed curve), which yield solutions with the same maximum value, overestimate the amplitude of the solitary waves in the discrete case (solid curve), while the P22 approximation (dotted curve) underestimates it, though the values it provides are closer to the ones for the discrete model. For smaller $|\beta|$, e.g., $\beta = -1$, the quasicontinuum models provide a good approximation of the relatively small amplitude of the discrete solution near the sonic limit but deviate from their discrete counterpart at larger velocities. For larger $|\beta|$, such as $\beta = -19/4$ and $\beta = -21/4$ corresponding to the bistable interactions, the models capture the overall trend of the amplitude-velocity relation in the discrete model, such as its near-linear form and nonzero sonic limit, but the quantitative difference in amplitudes is significant over the entire velocity range, though it decreases as the sonic limit is approached.

We now consider the strain profiles at various velocities shown in Fig. 8 and Fig. 9 for $\beta = -1$ and $\beta = -21/4$, respectively, and $\alpha = 4$. We first consider the local approximations. One can see that the CR model produces more narrow and taller waves, while the P22 approximation yields

waves that are wider than their discrete counterparts and have smaller amplitude. As expected due to the higher accuracy of the P22 model, it yields strain profiles that are overall closer to the ones for the discrete problem. Note that, while the waves have wider core regions in this case compared to both discrete problem and CR approximation, their decay at infinity is faster than that of the CR solutions [recall (31)], though it is slower than in the discrete case. Recall that in the sonic limit all three models yield the same algebraic decay (14) at infinity.

One can see that at smaller $|\beta|$ the CR and P22 models work very well in the near-sonic regime, where solutions have relatively small amplitude and decay slowly; see Fig. 8. The P22 model continues to work reasonably well at larger velocities. However, at larger $|\beta|$, including values that correspond to nonconvex interaction potentials, the solutions are strongly localized over the entire velocity range, and the two models yield solutions that deviate substantially from their discrete counterparts in the core region; see Fig. 9. They also completely miss the oscillations observed in the discrete case due to nonconvexity, as shown in the insets. We remark that the P22 solution at $V = 1.001$ in the upper left panel of Fig. 9 is triple-valued for $0.826 < \xi < 0.835$, due to an artifact of

the Padé approximation in this parameter regime, as explained in Sec. IV B.

Solitary waves for the GA model have the same amplitude as the CR model but are significantly wider and decay slower than for the other three models due to its poor approximation of the long-wave $k = 0$ limit. When solutions of the discrete model are sufficiently localized, which is the case for larger velocities at smaller $|\beta|$ and for the entire velocity range at larger $|\beta|$, the GA model does a good job of capturing the middle part of the wave, yielding a better approximation of its width in the discrete case than the two local models. But its solutions deviate considerably from their discrete counterparts near $\xi = 0$ and also at large $|\xi|$, due to the much slower decay.

V. CONCLUDING REMARKS

We considered a one-dimensional nonlinear lattice with interaction forces $f(w)$ that are sublinear near the undeformed state and include the case of bistable bonds. Using Fourier spectral numerical method, we constructed rarefactive solitary wave solutions propagating with supersonic velocities. These results are in excellent agreement with direct numerical simulations initiated by the computed waves, suggesting their stability. In contrast to the typical sonic delocalization, our solutions have a nontrivial Chapman-Jouguet sonic limit with nonzero energy and $O(1/\xi^2)$ decay at infinity.

We then investigated in detail two local quasicontinuum models that mimic some results of the discrete model, such as the overall trend of the amplitude-velocity relation and the nontrivial nature of the sonic limit, and predict the correct asymptotic behavior of the limiting solution at infinity. When $\beta = f''(0) < 0$ is sufficiently small, the models yield results that are also in a very good quantitative agreement with the discrete model at velocities that are close enough to the sonic limit. However, at larger $|\beta|$, which importantly includes the case of bistable interactions, solitary waves obtained from the quasicontinuum approximation deviate from their discrete counterparts in the core region for the entire velocity range due to their strongly localized nature. They also fail to capture some finer details of the solutions such as oscillations due to the combination of nonconvexity and advance-delay terms in the traveling wave equation for the discrete problem. An attempt to use a global approximation of the discrete operator instead of local expansion near the long-wave limit did not eliminate these shortcomings.

Our findings demonstrate that standard methods of approximating lattice solitary waves in the continuum setting are not in general appropriate in the case of bistable interactions, and new approaches need to be developed. In particular, this includes deriving an equation for the near-sonic rarefactive solutions that replaces the no longer relevant KdV equation in this setting. It is already clear that such an approximation must have a global character in order to capture a wider range of wavelengths, though it needs to be more sophisticated than the relatively simple form we considered in Sec. IV C. The challenge is to include enough terms in the Fourier space while preserving some degree of analytical transparency that would make such a description useful in providing insights about the discrete model.

[1] E. Fermi, J. Pasta, and S. Ulam, Technical Report, I, Los Alamos Scientific Laboratory Report No. LA-1940, 1955.

[2] N. J. Zabusky and M. D. Kruskal, Phys. Rev. Lett. **15**, 240 (1965).

[3] R. Hirota and K. Suzuki, Proc. IEEE **61**, 1483 (1973).

[4] T. Kofane, B. Michaux, and M. Remoissenet, J. Phys. C **21**, 1395 (1988).

[5] C. Coste, E. Falcon, and S. Fauve, Phys. Rev. E **56**, 6104 (1997).

[6] V. F. Nesterenko, *Dynamics of Heterogeneous Materials* (Springer, New York, 2001).

[7] B. Deng, P. Wang, Q. He, V. Tournat, and K. Bertoldi, Nat. Commun. **9**, 3410 (2018).

[8] B. Deng, V. Tournat, P. Wang, and K. Bertoldi, Phys. Rev. Lett. **122**, 044101 (2019).

[9] B. Deng, Y. Zhang, Q. He, V. Tournat, P. Wang, and K. Bertoldi, New J. Phys. **21**, 073008 (2019).

[10] H. Yasuda, Y. Miyazawa, E. G. Charalampidis, C. Chong, P. G. Kevrekidis, and J. Yang, Sci. Adv. **5**, eaau2835 (2019).

[11] S. Shrivastava, K. H. Kang, and M. F. Schneider, Phys. Rev. E **91**, 012715 (2015).

[12] M. Toda, *Theory of Nonlinear Lattices* (Springer, Berlin, 1981).

[13] G. Friesecke and J. A. D. Wattis, Commun. Math. Phys. **161**, 391 (1994).

[14] D. Smets and M. Willem, J. Funct. Anal. **149**, 266 (1997).

[15] A. Pankov and V. M. Rothos, Discr. Cont. Dyn. Syst. A **30**, 835 (2011).

[16] G. Friesecke and R. L. Pego, Nonlinearity **12**, 1601 (1999).

[17] G. Friesecke and R. L. Pego, Nonlinearity **15**, 1343 (2002).

[18] G. Friesecke and R. L. Pego, Nonlinearity **17**, 207 (2004).

[19] G. Friesecke and R. L. Pego, Nonlinearity **17**, 229 (2004).

[20] G. Iooss, Nonlinearity **13**, 849 (2000).

[21] E. McMillan, Nonlinearity **15**, 1685 (2002).

[22] A. Hoffman and C. Wayne, *Infinite Dimensional Dynamical Systems* (Springer, New York, 2013), pp. 185–192.

[23] G. Friesecke and K. Matthies, Physica D **171**, 211 (2002).

[24] M. Herrmann and K. Matthies, Nonlinearity **28**, 2767 (2015).

[25] M. Herrmann and K. Matthies, Trans. AMS **372**, 3425 (2019).

[26] D. Hochstrasser, F. G. Mertens, and H. Büttner, Physica D **35**, 259 (1989).

[27] J. C. Eilbeck and R. Flesch, Phys. Lett. A **149**, 200 (1990).

[28] J. English and R. Pego, Proc. AMS **133**, 1763 (2005).

[29] H. Xu, P. G. Kevrekidis, and A. Stefanov, J. Phys. A **48**, 195204 (2015).

[30] M. A. Collins, Chem. Phys. Lett. **77**, 342 (1981).

[31] Y. Gaididei, N. Flytzanis, A. Neuper, and F. G. Mertens, Physica D **107**, 83 (1997).

[32] V. F. Nesterenko, J. Appl. Mech. Tech. Phys. **24**, 733 (1983).

[33] P. Rosenau, Phys. Lett. A **118**, 222 (1986).

[34] P. Rosenau, Phys. Lett. A **311**, 39 (2003).

[35] J. A. D. Wattis, J. Phys. A **26**, 1193 (1993).

[36] J. A. D. Wattis, Phys. Scr. **50**, 238 (1994).

[37] J. A. D. Wattis, J. Phys. A **29**, 8139 (1996).

[38] P. Rosenau and A. Zilburg, Phys. Lett. A **381**, 87 (2017).

[39] K. R. Jayaprakash, Y. Starosvetsky, and A. F. Vakakis, Phys. Rev. E **83**, 036606 (2011).

[40] C. J. Lustri and M. A. Porter, SIAM J. Appl. Dyn. Syst. **17**, 1182 (2018).

[41] A. Vainchtein, Y. Starosvetsky, J. D. Wright, and R. Perline, Phys. Rev. E **93**, 042210 (2016).

[42] Y. Starosvetsky and A. Vainchtein, Mech. Res. Commun. **93**, 148 (2018).

[43] J. Wattis, Math. Eng. **1**, 327 (2019).

[44] L. Truskinovsky and A. Vainchtein, Phys. Rev. E **90**, 042903 (2014).

[45] L. Truskinovsky and A. Vainchtein, Physica D **389**, 24 (2019).

[46] L. Truskinovsky and A. Vainchtein (unpublished).

[47] A. Vainchtein, Wave Motion **83**, 12 (2018).

[48] J. L. Ericksen, J. Elasticity **5**, 191 (1975).

[49] I. Müller and P. Villaggio, Arch. Ration. Mech. Anal. **65**, 25 (1977).

[50] S.-C. Ngan and L. Truskinovsky, J. Mech. Phys. Solids **47**, 141 (1999).

[51] B. Fedelich and G. Zanzotto, J. Nonlinear Sci. **2**, 319 (1992).

[52] G. Puglisi and L. Truskinovsky, J. Mech. Phys. Solids **50**, 165 (2002).

[53] L. I. Slepyan, A. Cherkaev, and E. Cherkaev, J. Mech. Phys. Solids **53**, 407 (2005).

[54] L. Truskinovsky and A. Vainchtein, Phys. Rev. B **67**, 172103 (2003).

[55] L. Truskinovsky and A. Vainchtein, SIAM J. Appl. Math. **66**, 533 (2005).

[56] I. Benichou and S. Givli, Appl. Phys. Lett. **98**, 091904 (2011).

[57] I. Benichou and S. Givli, J. Mech. Phys. Solids **61**, 94 (2013).

[58] Q. Zhao and P. K. Purohit, J. Mech. Phys. Solids **92**, 176 (2016).

[59] M. Marder and S. Gross, J. Mech. Phys. Solids **43**, 1 (1995).

[60] L. I. Slepyan, *Models and Phenomena in Fracture Mechanics* (Springer-Verlag, New York, 2002).

[61] L. I. Slepyan and L. V. Troyankina, J. Appl. Mech. Tech. Phys. **25**, 921 (1984).

[62] E. Trofimov and A. Vainchtein, Cont. Mech. Thermodyn. **22**, 317 (2010); Erratum: **25**, 107 (2013).

[63] A. Vainchtein, J. Mech. Phys. Solids **58**, 227 (2010).

[64] A. Vainchtein and P. G. Kevrekidis, J. Nonlinear Sci. **22**, 107 (2012).

[65] H. Schwetlick and J. Zimmer, J. Nonlinear Sci. **17**, 1 (2007).

[66] S. Katz and S. Givli, Extr. Mech. Lett. **22**, 106 (2018).

[67] S. Katz and S. Givli, Phys. Rev. E **100**, 032209 (2019).

[68] L. D. Landau and E. M. Lifshitz, *Fluid Mechanics* (Pergamon Press, Oxford, 1987).

[69] Y. B. Zel'dovich and Y. P. Raizer, *Physics of Shock Waves and High-Temperature Hydrodynamic Phenomena* (Dover Publications, Mineola, NY, 2002).

[70] L. Truskinovsky, Arch. Ration. Mech. Anal. **125**, 375 (1994).

[71] J. Cuevas-Maraver, P. G. Kevrekidis, A. Vainchtein, and H. Xu, Phys. Rev. E **96**, 032214 (2017).

[72] H. Xu, J. Cuevas-Maraver, P. G. Kevrekidis, and A. Vainchtein, Philos. Trans. R. Soc. London A **376**, 20170192 (2018).